PHYSICS-BASED SAMPLING OF LOGNORMAL RESERVOIR WELL PRODUCTION/PRODUCTIVITY DISTRIBUTIONS

Peter Leary[1], Peter Malin[1] & Rick Starr[2]

[1]Institute of Earth Science & Engineering, University of Auckland, 58 Symonds Street, Auckland New Zealand

[2]Business School, University of Auckland, 12 Grafton Road, Auckland New Zealand

p.leary@auckland.ac.nz

Keywords: *Seismic emission tomography, geocriticality, fractures, spatial correlation, lognormality, statistical sampling.*

ABSTRACT

A large number of physical and social phenomena generate lognormal, 'long-tailed', or 'fat-tailed' population distributions. Such distributions cause considerable problems for statistical sample analysis because the underlying interactive processes giving rise to such system populations violate the central limit theorem. With no tendency for system processes to converge to normal distributions, the relation between sample data used for making decisions and actual system behaviour can be tenuous at best and catastrophic at worst. Crustal reservoirs are subject to high degrees of lognormality in well production/productivity. For reservoir engineering in general and geothermal reservoir engineering in particular, the breakdown of statistical sample analysis strongly impacts traditional reservoir modelling and greatly increases the risk/cost of reservoir drilling. However, unlike many/most systems having long-tailed populations, physical processes underlying reservoir flow lognormality are well constrained by empirical rules interpretable in terms that clearly indicate how and why reservoir engineers can sample their reservoir for flow structures at the spatial scales relevant to effective reservoir management. The physical elements of crustal reservoir flow heterogeneity and its appropriate spatial sampling scale are:

- Well log spatial fluctuation power spectra: $S(k) \sim 1/k$, $1/\text{km} < k < 1/\text{cm}$;
- Well core poroperm spatial fluctuation correlation: $\delta\varphi \sim \delta\log(\kappa)$;
- Well flow lognormality due to fracture-connectivity: $\kappa \sim \exp(\alpha\varphi)$, $\alpha >> 1$;
- Critical density ncrit grain-scale cement-bond-defect interactions leading to fluid percolation via long-range critical-state fracture-connectivity pathways;
- Seismic wave emission from dislocation slips at pressure-sensitive instabilities in large-scale flow-system fracture-connectivity structures.

Surface-seismic-array detection/mapping of large-scale *in situ* flow-system fracture-connectivity dislocation structures has been proven for the current generation of producing shale reservoirs. The same observational technology deployed at geothermal reservoirs can sample/map *in situ* flow structures at the spatial scales relevant to effective flow models and drill-site risk management.

1. INTRODUCTION

Prediction is very difficult, especially of the future.
(Attr Niels Bohr)

Drilling is about the future: Does the drill bit encounter economic fluids and flow?

Drilling is also:

- Expensive – 30 to 40% of the cost of a geothermal facility
- Chancy – Most wells, geothermal and otherwise, are sunk cost
- Necessary – No pay fluids without drilling

Observational procedures to improve drilling success deserve due consideration, particularly in the face of the extremely high rates of fluid flow required for commercial geothermal heat extraction. In interest of better drilling success, we restate the generic reservoir flow sampling problem in terms of the physical state of crust rather than in terms of an imposed statistical profile. Our terms of physical understanding of reservoir complexity expose a sampling problem which has no valid standard statistical solution, but does offer a valid physical solution.

The physics-versus-statistics distinction on well siting can be quickly highlighted:

- For physical reasons, it is far more efficient to base drilling decisions on sampling the reservoir at large scales for direct evidence of flow connectivity;
- For statistical reasons, it is far less efficient to base drilling decisions on sampling the reservoir at small scales to determine flow connectivity through statistical averaging.

The greater cost of physics-based large-scale observation is easily offset by greater drilling success arising from access to spatial information on *in situ* flow structure.

2. DEFAULT RESERVOIR STATISTICAL SAMPLING

The default view of *in situ* flow is typically expressed in terms of an REV or representative elementary volume [1-6]. At scales larger than an REV, it is generally supposed that, essentially by definition, fluids seep from REV to REV in a more-or-less reliably-connected spatially-averaged sense that is independent of the REV location in the reservoir. This view of reservoir flow can be quantified in terms of spatial correlations between pairs of (zero-mean unit-variance) porosity sequences $\Phi(r)$ and $\Phi(r+h)$ separated by distance h,

$$\Gamma(h) \equiv \langle \Phi(\underline{r})\Phi(r+h) \rangle \sim \Gamma_0 \exp(-h/\xi), \ \Gamma_0 > 0, \qquad (1a)$$

where the length parameter ξ represents the scale of the REV $\sim \xi^3$. The two end members values of spatial correlation function $\Gamma(h)$ are:

$$\Gamma(h) \sim 0, \ h >> \xi; \quad \Gamma(h) \sim \Gamma_0 > 0, \ h << \xi. \qquad (1b)$$

For reservoir sample separation large compared to the REV, $h >> \xi$, when sample spatial correlations vanish, it can be reliably assumed that N small-scale porosity samples $\Phi(r_n)$,

n = 1….N, average to a mean sample value that is a good estimate of the large-scale formation porosity. In a separate parallel logic, it is typically supposed that formation permeability associated with formation porosity is also adequately estimated by small sample permeability values.

The problem with default reservoir sampling view point expressing in Eqs. (1a-b) is that there is no evidence that the zero-correlation length scale ξ is small compared to formation/reservoir scales. Rather, the evidence is overwhelming that ξ in crustal rock is extremely large, $\xi \rightarrow \infty$ [7-9]. Large correlation lengths ξ mean that *in situ* spatial correlations $\Gamma(h) \sim \Gamma_0 > 0$ exist at all sample separations h, hence statistical averaging over small-scale spatial samples of reservoir properties does not reliably estimate large-scale property distributions within a formation or reservoir.

Sampling the physical properties of crustal rock requires statistics compatible with the *in situ* physical state. The appropriate statistical approach is direct observation of-large scale *in situ* flow structures most relevant to reservoir performance.

3. SAMPLING STATISTICS FOR SPATIALLY-CORRELATED RANDOMNESS OF *IN SITU* FLOW

Three empirical 'rules' constrain the spatial-correlation randomness of reservoir flow:

1. Spatial sequences of porosity $\varphi(s)$ along a wellbore are random but have a spatial frequency power spectrum that scales inversely with spatial frequency k, $S(k) \propto 1/k$, for scale lengths from cm to km [7-9].
2. Spatial sequences of well-core porosity φ_n are random but the logarithm of well-core permeability $\log(\kappa_n)$ is strongly correlated with porosity, $0.65 < \varphi_n \log(\kappa_n) > 0.9$, n = 1….N [11-12].
3. Crustal flow system permeability is random due to the random flow system porosity given by $\kappa \sim \exp(\alpha\varphi)$, with parameter $\alpha >> 1$; for normally distributed flow system porosity φ, the magnitude of α guarantees the distribution of flow system permeability κ is lognormal [13-14]

Fig 1 illustrates the spatial randomness of *in situ* flow conditioned by empirical rules 1-3. It is visually apparent that intersecting deep flow targets is better accomplished by remotely detecting the flow structures than by sampling small scale poroperm properties through drilling at sites chosen in reference to surface flow manifestations. While geothermal well siting is more directed than the 40-, 20- and 10 acre arbitrary siting of many/most oil/gas field wells, exploration and development drilling at, say, Ohaaki, Ngawha, Kawerau and Rotokawa geothermal sites in New Zealand using surface information remains a highly unreliable guide to deep flow structures [27-30]. More logical is to detect the large-scale *in situ* flow connectivity structures illustrated in Fig 1:

- By Rule 1, important flow structures occur at the *largest scale*, hence sampling should occur at larger scales;
- By Rule 2, drill-target flow is defined by large-scale *flow connectedness*, which should be the focus of observation;
- By Rule 3, large-scale flow structures are *rare and must be specifically observed* rather than statistically inferred.

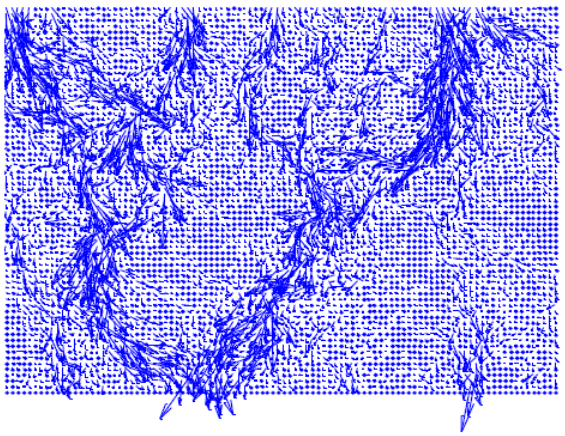

Figure 1: Flow vectors of a 2D porous medium that obeys the empirical 'rules' 1-3 of §3. Spatial correlation of *in situ* fractures leads to large-scale spatially-dependent fracture-connectivity structures. Such spatial-dependence is a direct contradiction of spatial independence that is characteristic of many concepts and models of *in situ* flow [1-6].

4. THE CRUSTAL 'CRITICAL STATE' UNDERLYING SPATIALLY-CORRELATED LONG-RANGE *IN SITU* FLOW CONNECTIVITY STRUCTURES

The physical state of crustal rock that gives rise to the observed empirical rules operates at the grain scale [7-9]. Tough mineral grains are bonded by weak cements. In the presence of finite strain induced by on-going tectonic deformation of the crust, intact cement bonds rupture to create grain-scale defects that allow passage of *in situ* fluids. From percolation theory we know that at a 'critical' density of such cement bond defects there is a high probability that a defect-connectivity pathway spans a given crustal volume [7-9]. Such large-scale percolation pathways occurring at crustal scales give rise to the power-law scaling empirical rule (1) and are the natural drilling targets for exploiting reservoirs.

Empirical rule (2) can be understood in the same physical terms. A number of grain-scale defects n in a crustal volume have a degree of defect connectivity which increases with defect number n in proportion to the factorial $n!$. The mathematical relation between n and $\log(n!)$, $log(n!) \sim nlog(n) - n$, is equivalent to empirical rule (2), giving a picture of fluid flow by grain-scale percolation in proportion to the number of combinations, $n!$, in which n defects can be linked within a crustal volume. The logarithm in (2) gives rise to the lognormal-skew nature of *in situ* permeability distributions (3), to which we can give a physical interpretation that fracture connectivity controls the ease with which *in situ* fluids flow along fracture-connectivity pathways at all scales. Lognormal-like skew of *in situ* flow systems thus naturally emerges from widely-attested physical properties of crustal rock [7-14].

The crustal 'critical state' is dynamic rather than static physical in nature, with fracture-connectivity being locally sensitive to small changes in fluid pressure. It has been long observed that small changes in the fluid pressure of crustal reservoirs lead systematically to discernable seismic emissions (including large-scale earthquakes) [15-18]. Recent detailed seismic monitoring investigations of reservoirs subject to *in situ* pressure changes through fluid depletion and/or hydrofracture operations show that small scale events occur preferentially along large-scale percolation fracture-connectivity pathways [19-22]. Systematic detection of such incidental acoustic emissions leads to reliable, repeatable, and physically interpretable *in situ* flow structure maps within a reservoir.

5. SEISMIC EMISSIONS IN SPATIALLY-CORRELATED LONG-RANGE *IN SITU* FLOW SYSTEMS

An active heat-transporting convective geothermal system is perhaps the ideal crustal volume in which to study natural seismic emissions generated by *in situ* flow. Fig 2 gives a 3 dimensional representation of the *in situ* spatial porosity/defect heterogeneity arising from empirical rules 1-3 and generating the long-range spatially-correlated flow-connectivity illustrated in Fig 1. Within the reservoir volume at depth below the crustal surface, some portions have higher porosity/defect density (light green clusters) and some have lower porosity/defect density (dark/blue-green clusters). The spatial correlations of the crustal defects is prescribed by spectral scaling relation (1). In line with empirical relations (2)-(3) and Fig 1 flow connectivity illustration, light green portions of the crustal volume are associated with greater well productivity, and dark/blue-green regions with lesser well productivity.

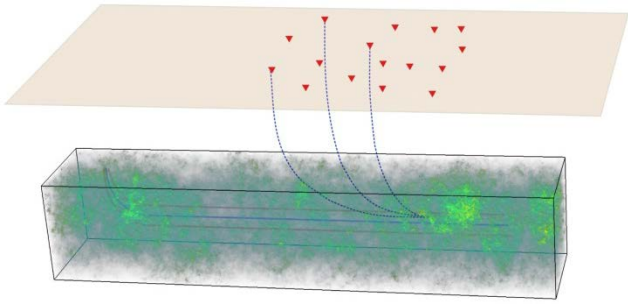

Figure 2: A generic crustal volume of nominal dimensions 1km in length and 200m in cross-section at arbitrary depth below a surface seismic array represented by inverted triangles in red. The distribution of green tints within the crustal volume represents spatially correlated variations in porosity in accord with well-log spectral empirics (1), $S(k) \propto 1/k^{\beta}$, $\beta \sim 1$, ~1/cm < k < ~1/km. Permeability heterogeneity within the volume is fixed by well-core empirics (2), $\delta\varphi \propto \delta log(\kappa)$. Fluid flow within the crustal volume follows from Darcy's equation $v(x,y,z) = \kappa(x,y,z)/\mu\nabla P(x,y,z)$. Fluid pressure/flow at poroperm points in the volume give rise to seismic-slip instabilities which emit seismic waves indicated by dashed blue lines and detected by surface seismic sensors [19-22].

Seismic emission/detection in the Fig 2 reservoir volume is indicated by blue dotted lines connecting *in situ* sources to surface sensors (red triangles). With a sufficient number of surface sensors and a long enough recording time, the very low level seismic events associated with *in situ* pressure-disequilibrium flow can be extracted from seismic background and back-traced to their spatial origin. This process is called "seismic emission tomography" (SET) [19-22]. Figs 3-4 illustrate the SET multi-channel seismic data analysis that can locate reservoir active flow regions suitable as drilling targets.

Small sub-noise seismic events registered on many seismic channels can be detected by systematically combing through the multi-channel data illustrated in Fig 3 for a 9x9-sensor surface seismic array illustrated as red triangles in Fig 2. Each of the nine panels represents the arrival of seismic energy at nine sensors. For a given interval of seismic data recording time – say 100 milliseconds – each sensor records background seismic activity which may, or may not, include a small seismic event arrival from the reservoir. Fig 3 shows one such arrival across the 9 x 9 sensor array (for visual clarity, the seismic arrivals are shown without background seismic noise that would otherwise overprint the signal).

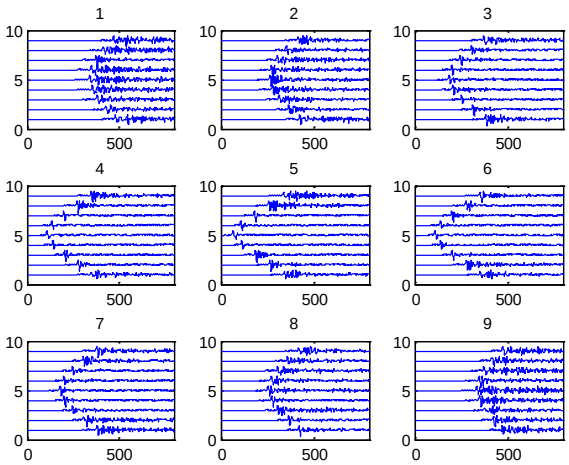

Figure 3: A snap-shot of a long temporal sequence of seismic data recorded by a 9 x 9 array of surface seismic sensors arising from a single source at depth in the reservoir volume as depicted in Fig 2. The array data display shows the event without background noise; in a realistic simulation of SET data processing, each signal is buried in background noise ten or more times the magnitude of the largest event signal.

Events with arrivals at multiple sensors illustrated in Fig 3 are identified and back-located in space by the following SET data processing logic:

- Assume an event occurred in a particular node or voxel within the reservoir volume;
- Using a pre-computed travel-time table, look up the travel time from the particular node to each sensor, and shift each seismogram according to the computed travel time so that the expected arrival occurs at the earliest time within the window;
- Sum/stack all such time-shifted seismograms to evaluate one of three options:
  - If the event occurred in the given node/voxel, each time-shifted initial seismic motion will be aligned at

the beginning of the traces of all sensors, and the summed/stacked seismogram can have an initial arrival as shown in the upper trace of Fig 4;
  - If the event occurred near the given node/voxel, the time-shifted initial seismic motions will be partially aligned for some but not all sensors;
  - If the event occurred away from the given node/voxel, the time-shifted initial seismic motions will not be aligned and the summed/stacked seismogram will have no statistically significant peak as in lower trace of Fig 4;
- If the summed/stacked seismogram has a signal of sufficient strength, add a weighted 'semblance' value to the given node/voxel; otherwise add nothing to the node/voxel;
- Repeat the time-shift winnowing sequence for each node/voxel in the crustal model until all nodes/voxels are processed.
- Move to a new time-interval and repeat the above process.

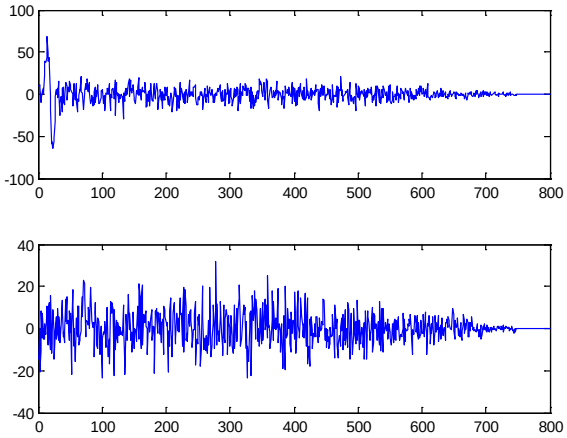

Figure 4: SET data processing involves shifting each of the Fig 3 traces back and forth along its time axis according to the following logic: (a) If trace X contains a signal from a hypothetical event at source location Y, then if that trace is shifted by T_{XY} units in time, T_{XY} = the travel-time between source sensor X and source location Y, the signal should be shifted to the beginning of record; (b) Summing all traces X time shifted by amounts T_{XY} for an actual source at location Y adds traces constructively to produce an identifiable net signal (upper trace); (c) Summing all traces X time shifted by amounts T_{XY} for an non-existent source at location Y adds traces destructively to produce a noise sequence (lower trace). SET data processing repeats the trace-by-trace time-shift procedure for every small time window in a recording sequence for every source location with a 3D mesh representation of the reservoir. A typical SET scan may involve many thousands of time windows and source-point mesh nodes, and hundreds of sensors.

The processed data output from the surface seismic array recordings are given 'semblance' values for each node/voxel of the crustal volume model. The final semblance counts are the total magnitudes of the summed/stacked traces given as the initial spike at the Fig 4 upper-panel synthetic trace. The higher the spike over background noise, the stronger is the imaging signal and the more active is the crustal node/voxel site.

6. SET EVENT LOCATION IN SHALE RESERVOIRS

SET data processing of surface seismic array to locate sub-noise reservoir slip events associated with *in situ* fluid flow pathways has been validated at shale gas/oil reservoir production sites [19-22]. Fig 5 shows a color-coded spatial semblance plot for two 1.5km-long horizontal wells in a shale reservoir (wellbore traces appear as thin red horizontal lines across the figure). Seismic events in the aftermath of a series of wellbore hydrofracture stimulations were recorded by a permanent array of subsurface seismic sensors overlying a producing shale reservoir at 3km depth as illustrated in Fig 2. The Fig 5 color-coded induced-event locations derived from SET processing show lower-semblance values as the violet/blue end of the color spectrum, and higher-semblance values as the red end of the spectrum. The spatial resolution of the SET locations is on the order of 10m; the radial extent of the SET images is 50-60m.

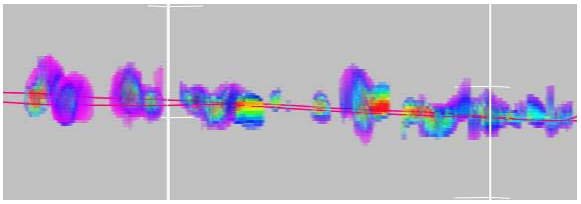

Figure 5: Shale reservoir wellbore SET semblance sequence along wellbore. Colors denote spatial distribution of semblance magnitude. Warm colors are higher semblance; cool colors are lower semblance. Note the similarity of spatial heterogeneity with that of Fig 2.

From Fig 5 semblance data, we see that wellbore event stimulation signals associated with fluid production

- are strong near the wellbore and decrease in strength away from the wellbore;
- vary in strength along the wellbore.

We can model the Fig 5 field data radial and axial strength distributions and spatial heterogeneity by considering *in situ* flow from the reservoir formation into the stimulation fracture-plane and from the fracture-plane into the wellbore. Such a flow model applied to wellbore time-evolution fluid production curves gives two effective diffusion constants for the reservoir: (i) a diffusion constant for fracture-borne flow into the wellbore; and (ii) a diffusion constant for formation flow into the fracture. Fig 6 shows a time-evolution production curve for oil (blue) and gas (red) matched by a model curve (smooth black line); production erratics are due to wellbore flow operations.

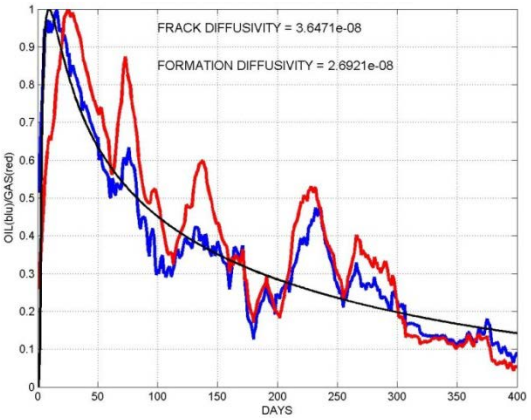

Figure 6: Time-evolution production curve for oil (blue) and gas (red) matched by a model curve (smooth black line); production erratics are due to wellbore flow operations.

Fig 7 shows model fluid flow radial and axial variability for a series of 12 planes normal to a wellbore along the length of the Fig 2 crustal simulation volume. As with the Fig 5 SET semblance distributions along a shale reservoir wellbore, the model wellbore-centric fluid flow magnitudes vary radially and axially:

- Flow strongest near the central wellbore, decreasing away from the wellbore;
- Flow variation at the 12 fracture planes along the wellbore axis;
- Instances of strong flow as seen in the red-coded semblance values in Fig 5.

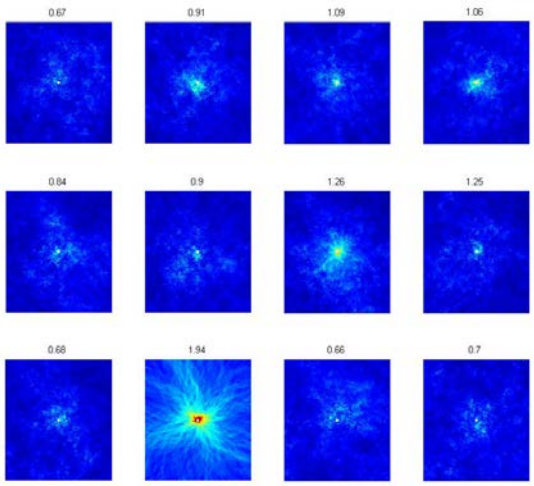

Figure 7: Model fluid flow radial and axial variability for a series of 12 planes normal to a wellbore along the length of the Fig 2 crustal simulation volume. In common with, but not conditioned by the observed Fig 5 SET semblance distributions along a shale reservoir wellbore, the model wellbore-centric fluid flow magnitudes vary radially and axially as a function of the stochastic nature of *in situ* poroperm spatial fluctuations.

The collective flow computed for poroperm stimulation structures such as shown in Fig 7 can be computed, but such computations are difficult to compare decisively with collective wellbore flow as measured in Fig 6 field data.

7. APPLICATION OF SEISMIC EMISSION TOMOGRAPHY IN GEOTHERMAL SYSTEMS

SET processing of surface seismic data recorded over a producing shale reservoir identified *in situ* fracture-flow-connectivity structures indicated by red lines in the 3km x 3km sections shown in Fig 8. The inferred red-line fracture-connectivity flow structures were mapped on the basis of seismic array site monitoring in advance of well stimulation (but not well drilling). A hydrofracture sequence conducted in a 1km horizontal wellbore at the center of the section produced an initial signal (slight smudge at center of left-hand section) which grew into further signal activity at the original conductivity structure plus activating a remote fracture-connectivity structure (center section) and culminated in still further activity in the center structure with activity at three remote structures (right-hand section).

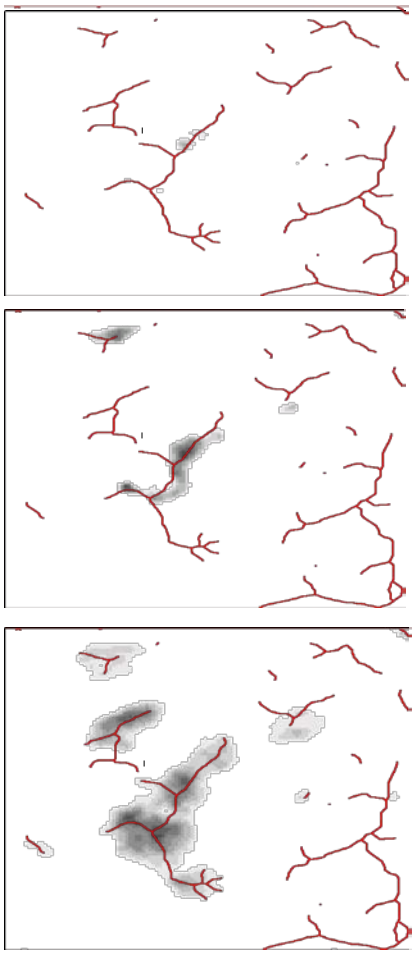

Figure 8: A hydrofracture sequence conducted in a 3km by 3km reservoir section from a 1km horizontal wellbore at the center of the section. The initial SET signal is slight smudge at center of top section; at subsequent times, SET signal activity at the original conductivity structure plus at remote fracture-connectivity structures; the time sequence culminates in further activity in the center structure with activity at three remote structures (bottom section). Noteworthy is that fracture stimulation did not affect the rightmost mapped connectivity structures; the latter fracture set would be a logical target for further drilling.

It is noteworthy in the Fig 8 hydrofracture sequence that the fracture stimulation activity of some of the connectivity structures did not affect the rightmost mapped connectivity structures. One can immediately infer the degree of fracture connectivity within and between the mapped connectivity structures. The lack of hydrofracture stimulation connectivity across the section implies that an addition well be drilled in the lower-right non-connectivity sector. The km-scale on which this signal activity is observed illustrates a degree of spatial extent and spatial resolution that would apply to geothermal systems.

The basis for achieving the exhibited shale reservoir SET spatiotemporal image resolution of Figs 5 and 7 is an adequate velocity model of the reservoir volume. Only with adequate velocity structure information can the SET analysis process accurately align the small signals emitted by pressure-disturbed fluid-active fracture connectivity structures at reservoir depths. Most shale reservoir prospects have surface seismic sections which return detailed velocities models; these models can be further refined for a set of surface seismic array stations by recording perforation shots conducted during wellbore completions. This level of velocity information is not available to geothermal systems; pyroclastic flow sequences are notoriously difficult to image with seismic reflectivity methods, and well completion perforations are not the integral part of geothermal production that they are in shale reservoir production. Nonetheless, methods exist to probe complex velocity structures [23-25]. As a counter to the complexity of their seismic velocity structures, geothermal fluid flow systems are vastly more active than are those of shale reservoirs, and the spatial resolution required for usefully guiding the drill bit to flow-productive areas of the overall geothermal system is substantially less than that relevant to hydrofracturing operations important to shale reservoir production.

8. DISCUSSION: RESISTING THE TEMPTATION TO ASSUME EVENT INDEPENDENCE WHEN PREDICTING THE FUTURE

Statistical approaches to risk and/or uncertainty in predicting future events generally have at their core the assumption that a sample of events somehow usefully represents the entirety of events. Where it is conceded that the full range of outcomes cannot be known, it is often assumed that a handful of known outcomes can help define risk and reduce uncertainty. This assumption is accurate in many circumstances. In games of chance or for engineering materials, a regularity or uniformity exists that allows the future to be a good guide to the past: 4 x 13 distinct playing cards in a deck, six distinct sides to a die, two sides to a coin, rigid controls on the density, strength, composition, hardness, temperature of various engineering processes. Risk and uncertainty exist, but are manageable on the basis of relatively straightforward sampling tactics over a uniform event field.

In contrast, suppose that shuffling a deck of cards is systematically faulty, in that cards of a suit have a strong tendency to associate with other cards of that suit. Suddenly within a game there can be suit-specific trends that have no connection with uniform event sampling. Uncertainty and risk rise and efficiency drops. Once the phenomena of hidden trends within shuffled decks become apparent, there will ensue attempts to recognize trends, but history indicates that such attempts are simply variations on the general theme of some sort of uniformity or regularity [26]. For instance, enough observation may indicate that the two of spades tends to associate with the three of spades, whence the risk/uncertainty tables will be adjusted accordingly as if the pairing of the two and three of spades is itself a new form of regularity or independent event that can be used to predict future events on the basis of occurrence within a sample.

The tendency to work for and believe in uniformity or regularity of independent events has another manifestation relevant to *in situ* flow. Rare conjunction of events, as for instance associated with accidents, are often discounted in probability because their chance of occurrence is estimated as the product of the chance of each element of the conjunction. This is an accurate expectation if the conjunctive events are truly independent, but in many accidents the conjunctive events are dependent rather than independent [26]. In the case of *in situ* flow systems, large-scale dominant flow structures may be rare (lognormally distributed) but they are far, far more common that would be expected if all fracture-connectivity conjunctions were taken as independent events.

The empirical physics of *in situ* flow structures speaks directly to the matter of dependent events that comprise a flow system. The first two empirical rules of crustal rock noted in §3,

a) Spatial sequences of porosity $\varphi(s)$ along a wellbore are random but have a spatial frequency power spectrum that scales inversely with spatial frequency k, $S(k) \propto 1/k$, for scale lengths from cm to km;
b) Spatial sequences of well-core porosity φ_n are random but the logarithm of well-core permeability $\log(\kappa_n)$ strongly correlated with porosity, $0.65 < \varphi_n \log(\kappa_n) > 0.9$, $n = 1 \ldots N$;

give rise to two physical/mathematical truths about *in situ* flow. First, if the fracture connectivity events that comprise *in situ* flow systems were spatially independent, the spatial frequency power spectrum of a wellbore trace would have the specific form of 'white noise', $S(k) \propto 1/k^0 \sim constant$, instead of the observed form $S(k) \propto 1/k^1$ as given in a). Second, as indicated above, the fracture-connectivity aspect of *in situ* flow arises directly from b) by counting the number of ways spatially correlated fractures can connect. Consider a unit volume of rock containing n fractures; the number of fracture-connections is proportional to the number of ways that n fractures can connect, $n! \equiv n\,(n\text{-}1)\,(n\text{-}2)\,(n\text{-}3)\ldots\ldots 1$. A neighbour volume with $n+\delta n$ grain-scale fractures has $(n+\delta n)!$ ways to connect. The number of fractures in a volume element is proportional to the porosity of the volume element, $n \propto \varphi$, and the number of fracture connections is proportional to the permeability of the element, $n! \propto \kappa$. This is because grain-scale fractures are more likely to occur where rock is porous and subject to greater strain than elsewhere; and fracture connectivity essentially defines what we mean by permeability. Stirling's formula, $n! \sim (n/e)^n \sqrt{2\pi n}$, expressed as $log(n!) \sim n\,log(n) - n$ returns physical empirics b) as the difference in the logarithm of permeability proportional to the difference in porosity, $\delta log(n!) = log((n+\delta n)!) - log(n!) \propto n + \delta n - n = \delta n$.

Physical/mathematical expression of empirical properties a) and b) associated with *in situ* flow indicates the fundamental importance of spatial correlation dependence

of *in situ* fracture events in determining the flow properties of rock. It is grossly at odds with physical reality to express flow-system statistics in terms of independent events. At the same time, the empirical lognormality of *in situ* flow system populations in crustal rock indicates that large-scale flow systems are rare (but not as rare as they would be if the flow systems were built of independent spatial occurrence of fractures, which is the default assumption about reservoir flow typically associated with geostatistical applications [1-6]). Trying to find rare spatial occurrences of significant *in situ* flow systems determined by fundamentally spatially-dependent physical processes by means of expensive/risky drilling based on sampling strategies rooted in the statistics of independent events is highly inefficient.

9. SUMMARY/CONCLUSIONS

The potential for locating fracture-connectivity flow structures in natural geothermal flow systems is great. The flow-signal in geothermal systems is probably one or more orders of magnitude greater for geothermal flow than for shale reservoir stimulated flow, and the spatial resolution needed to usefully guide the drill bit to the most promising areas is sizably less than that needed to guide shale reservoir hydrofracture operations. Finally, the effective/operational cost a geothermal well is at least an order of magnitude greater than that of a shale reservoir well. The play of these factors compensates for the challenges of acquiring adequately resolved velocity structure models with which to conduct SET analysis of surface seismic array recording data. Establishing an SET-based methodology for increasing net geothermal well productivity would likely

- bring new more marginal fields on line;
- enhance the productivity of existing fields;
- extend the life of existing fields by enabling effective location of suitable sites for re-injection wells.

REFERENCES

[1] Kozeny J (1927) Ueber kapillare Leitung des Wassers im Boden: Sitzungsberichte Wiener Akademie, v. 136, no. 2a, p.271–306; Wasserkraft u Wasserwitschaft, 22, 67 (1927a) and 22, 86 (1927b).

[2] Carman PC (1937) Fluid flow through granular beds, Trans . Inst . Chem. Engrs ., London, v. 15, p. 150-166. Institute of Chemical Engineers, London, v. 15, 150-166.

[3] Biot MA (1941) General theory of three-dimensional consolidation, *Journal of Applied Physics*, v. 12, no. 2, p. 155-164.

[4] Bear J & Bachmat Y (1984) Transport Phenomena in Porous Media Basic Equations, *Fundamentals of Transport Phenomena in Porous Media*, J. Bear & M. Y. Corapcioglu, eds., Martinus Nijhoff BV, The Hague, Netherlands,.pp 3 – 62.

[5] Ingebritsen SE, Sanford WE & Neuzil CE (2006) *Groundwater in Geologic Processes*, Cambridge University Press, 536p.

[6] Mavko G, Mukerji T & Dvorkin J (2009) *The Rock Physics Handbook*, Cambridge University Press, 511p.

[7] Leary PC (1997) Rock as a critical-point system and the inherent implausibility of reliable earthquake prediction, *Geophysical Journal International* 131, 451-466.

[8] Leary PC (2002) Fractures and physical heterogeneity in crustal rock, in *Heterogeneity of the Crust and Upper Mantle – Nature, Scaling and Seismic Properties*, J. A. Goff, & K. Holliger (eds.), Kluwer Academic/Plenum Publishers, New York, 155-186.

[9] Stauffer D & Aharony A (1994) *Introduction to Percolation Theory*, Taylor & Francis, pp192.

[10] Leary PC & Al-Kindy F (2002) Power-law scaling of spatially correlated porosity and log(permeability) sequences from north-central North Sea Brae oilfield well core, *Geophysical Journal International* 148, pp426-442.

[11] Leary P, Pogacnik J & Malin P (2012) Fractures ~ Porosity --> Connectivity ~ Permeability --> EGS Flow Stimulation, *Proceedings 36th Geothermal Resources Council 36th Annual Conference*, 30 Sep – 3 Oct, Reno NV.

[12] Leary PC, Malin PE, Ryan GA, Lorenzo C & Flores M (2013) Lognormally distributed K/Th/U concentrations – Evidence for geocritical fracture flow, Los Azufres geothermal field, MX, *Proceedings Geothermal Resources Council 37th Annual Conference*, 29 Sep – 3 Oct, Las Vegas NV.

[13] Leary P, Malin P, Pogacnik J, Rugis J, Valles B & Geiser P (2014) Lognormality, $\delta\kappa \sim \kappa\, \delta\varphi$, EGS, and all that, *Proceedings 39th Stanford Geothermal Workshop*, February 24-26 2014, Stanford University, CA.

[14] Leary P, Pogacnik J & Malin P (2012) Computational EGS -- Heat transport in 1/*f*-noise fractured media, *Proceedings 37th Stanford Geothermal Workshop*, Stanford University.

[15] Simpson DW & Negmatullaev SK (1980) Induced seismicity at Nurek Reservoir, Tadjikistan, USSR, *Bulletin of the Seismological Society of America* 70, 1561-1586.

[16] Simpson DW, Leith WS & Scholz CH (1988) Two types of reservoir-induced seismicity, *Bulletin of the Seismological Society of America* 78, 2025-2040.

[17] Segall P (1989) Earthquakes triggered by fluid extraction. Geology 17(10), 942–946.

[18] Ziv A & Rubin AM (2000) Static stress transfer and earthquake triggering: No lower threshold in sight?, *Journal of Geophysical Research* 105, 631-642.

[19] Kugaenko Y, Saltykov V, Sinitsyn V & Chebrov V (2005), Passive Seismic Monitoring in Hydrothermal Field: Seismic Emission Tomography, *Proceedings World Geothermal Congress* 2005, Antalya, Turkey, 24-29 April.

[20] Geiser P, Vermilye J, Scammell R & Roecker S (2006a) Seismic Emission Tomography 1: Seismic used to directly map reservoir permeability fields, *Oil & Gas Journal* 104, no. 46 6pp.

[21] Geiser P, Vermilye J, Scammell R & Roecker S (2006b) Seismic Emission Tomography - 2: Seismic used to directly map reservoir permeability fields, *Oil & Gas Journal* 104, no. 47, 6pp.

[22] Geiser P, Lacazette A & Vermilye J (2012) Beyond 'dots in a box': an empirical view of reservoir permeability with tomographic fracture imaging, *First Break* 30, p. 63-69.

[23] Louie JN, Pullammanappallil SK & Honjas W (2011) Advanced seismic imaging for geothermal development, *Proceedings New Zealand Geothermal Workshop* 21 - 23 November 2011, Auckland, New Zealand;

[24] Pullammanappallil SK & Louie JN (1994) A generalized simulated-annealing optimization for inversion of first arrival times, *Bulletin of the Seismological Society of America, 84*, 1397-1409;.

[25] Pullammanappallil S, Honjas W, Unruh J & Monastero F (2001) Use of advanced data processing techniques in the imaging of the Coso geothermal field, *Proceedings 26th Workshop Geothermal Reservoir Engineering*, Stanford University January 29-31.
[26] Kruskal W (1988) Miracles and statistics: The casual assumption of independence, *Journal American Statistical Association* 83, No. 404, 929-940.
[27] Grant MA (2009) Optimization of drilling acceptance criteria, *Geothermics* 38, 247–253.
[28] Bignall G & Milicich SD (2012) Kawerau Geothermal Field, *GNS Science Report 2012/33*, 28pp.
[29] Quinao JJ & Sirad-Azwar L (2012) Correlation of reservoir monitoring and continuous production data to interpret unexpected well behavior in Rotokawa, Proceedings New Zealand Geothermal Workshop, 19–21 November, Auckland, New Zealand.
[30] Sewell SM, Cumming W, Bardsley CJ, Winick, J, Quinao J, Wallis IC, Sherburn S, Bourguignon S & Bannister S (2013) Interpretation of microearthquakes at the Rotokawa geothermal field, 2008 to 2012, Proceedings 35th New Zealand Geothermal Workshop, 17–20 November, Rotorua, New Zealand.